UC Berkeley

Title

All-Liquid Reconfigurable Electronics Using Jammed MXene Interfaces

Permalink

https://escholarship.org/uc/item/2c2564xg

Journal

Advanced Materials, 35(13)

ISSN

0935-9648

Authors

Popple, Derek
Shekhirev, Mikhail
Dai, Chunhui
et al.

Publication Date

2023-03-01

DOI

10.1002/adma.202208148

Peer reviewed

All-Liquid Reconfigurable Electronics Using Jammed MXene Interfaces

Derek Popple, Mikhail Shekhirev, Chunhui Dai, Paul Kim, Katherine Xiaoxin Wang, Paul Ashby, Brett A. Helms, Yury Gogotsi, Thomas P. Russell,* and Alex Zettl*

Rigid, solid-state components represent the current paradigm for electronic systems, but they lack post-production reconfigurability and pose ever-increasing challenges to efficient end-of-life recycling. Liquid electronics may overcome these limitations by offering flexible in-the-field redesign and separation at end-of-life via simple liquid phase chemistries. Up to now, preliminary work on liquid electronics has focused on liquid metal components, but these devices still require an encapsulating polymer and typically use alloys of rare elements like indium. Here, using the self-assembly of jammed 2D titanium carbide ($Ti_3C_2T_x$) MXene nanoparticles at liquid–liquid interfaces, "all-liquid" electrically conductive sheets, wires, and simple functional devices are described including electromechanical switches and photodetectors. These assemblies combine the high conductivity of MXene nanosheets with the controllable form and reconfigurability of structured liquids. Such configurations can have applications not only in electronics, but also in catalysis and microfluidics, especially in systems where the product and substrate have affinity for solvents of differing polarity.

1. Introduction

Modern electronics rely almost exclusively on solid-state components, from solid, metal wire interconnects, rigid thin-film resistors, and capacitors to semiconductor diodes, transistors, and related elements. While this approach lends itself to impressive integration capabilities, it poses increasingly important challenges to reconfigurability and recyclability. Indeed, extracting limited-supply metals from discarded electronics is an ever-growing worldwide concern.[1–3]

The rigid nature of solid-state electronics yields mechanical and temporal stability, but this very stability is the principal drawback in full life-cycle reuse. Numerous recent advances in solid-state flexible electronics[4–6] employing, for example, flexible polymer substrates and film components offer applications advantages as wearable, flexible electronics. Still, they do little to address the reconfigurability or recyclability problems. Other approaches including plastic composites or hydrogels utilize strong intermolecular forces or electrostatic interactions to facilitate impressive reconfigurability.[7,8] However, the crosslinked nature of these systems may make it difficult to separate the constituents at the end of life, again complicating recycling of the materials.

D. Popple
Department of Chemistry
University of California Berkeley
Berkeley, CA 94720, USA

D. Popple, C. Dai, K. X. Wang, A. Zettl
Department of Physics
University of California Berkeley
Berkeley, CA 94720, USA
E-mail: azettl@berkeley.edu

D. Popple, C. Dai, P. Kim, P. Ashby, B. A. Helms, T. P. Russell, A. Zettl
Materials Sciences Division
Lawrence Berkeley National Lab
1 Cyclotron Road, Berkeley, CA 94720, USA
E-mail: russell@mail.pse.umass.edu

D. Popple, A. Zettl
Kavli Energy NanoSciences Institute at the University of California at Berkeley and the Lawrence Berkeley National Laboratory
Berkeley, CA 94720, USA

M. Shekhirev, Y. Gogotsi
Department of Materials Science & Engineering and A. J. Drexel Nanomaterials Institute
Drexel University
Philadelphia, PA 19104, USA

P. Ashby, B. A. Helms
Molecular Foundry Division
Lawrence Berkeley National Lab
1 Cyclotron Road, Berkeley, CA 94720, USA

T. P. Russell
University of Massachusetts, Amherst
Amherst, MA 01003, USA

ADVANCED
SCIENCE NEWS

www.advancedsciencenews.com

ADVANCED
MATERIALS

www.advmat.de

The creation of electronic devices and architectures that capitalize on the exceptionally pliable nature of liquids provides an attractive but virtually unexplored alternative paradigm. Past work has focused on using room-temperature liquid metals to demonstrate devices and rudimentary circuits.[9–13] These approaches use the metallic properties of liquid metal alloys for good electrical transport and typically use polymer encapsulation to give the devices a useful form-factor. While showing promise, such configurations still employ conventional solid-state electronics architectures requiring a solid substrate or encapsulating medium to provide form. Also, the room temperature liquid metals are largely limited to indium and gallium alloys, which have many limitations. As a result, more work is needed to develop complementary material systems that provide electrical transport but are free from the limitations of solid substrates or encapsulation.

2. Approach

We explore an approach where the entirety of the electronics platform is liquid-based. Instead of a silicon chip host substrate, the host medium is an insulating liquid whose viscosity may be tunable. Conducting pathways are created by electrically conductive nanoparticles self-assembled and jammed at liquid–liquid interfaces.[14] In principle, interconnects, resistors, capacitors, inductors, switches, diodes, transistors, etc., can be created via combinations of jammed nanoparticle interfaces. As such, functions are easily reconfigured post-production, and the constituent elements are easily extracted and recycled at the end-of-lifetime using conventional liquid chemical processes. In addition, the ability to electrify the interface between liquids provides opportunities to create electrically active fluidic devices, which are difficult to achieve using previously demonstrated reconfigurable or liquid metal electronics.

To create the jammed interface, nanoparticles and ligands are dissolved in separate immiscible phases.[14] If the ligands and nanoparticles have complementary functionalities, these components form a nanoparticle–surfactant complex that can tether the nanoparticle to the liquid–liquid interface. The interface will continue to saturate with nanoparticle–surfactant complexes, creating a packed layer of the complexes while reducing the interfacial tension between the two liquids. This phenomenon has been exploited to demonstrate liquid–liquid 3D printing of structured (non-electronic) liquids,[15–18] allowing the design, construction, and repeated manipulation of complex geometries. In addition, there have been demonstrations of structured liquids showing magnetism, catalysis, and reconfiguration.[16,19,20] This immediately provides a rich toolbox for the construction of jammed nanoparticle interfaces.

The key to unlocking applications in electronics is a realization of an electrically conductive interface created using intrinsically electrically conductive nanoparticles that, upon jamming, form a stable conductive network. MXene nanosheets[21,22] are excellent candidates due to their high electrical conductivity, hydrophilicity, and ability to self-assemble at oil–water interfaces in the presence of a ligand with complementary charge.[17,23,24] The MXenes are 2D transition metal carbides, nitrides, and carbonitrides, which are typically synthesized by selective chemical etching of 3D MAX phase precursors (where M is an early transition metal, A is a group 13 or 14 element, and X is C and/or N), leaving behind 2D nanosheets with O, OH, F or other surface terminations.[25] MXenes possess a high density of states at the Fermi level and a high concentration of carriers, which makes them more conductive compared to typical carbon nanomaterials. In particular, $Ti_3C_2T_x$ has demonstrated conductivity of 10 000–20 000 S cm^{-1} and a very high breakdown current.[26] These properties can be maintained in multilayer films and composites.[27] A highly negative surface charge makes the MXene nanosheets readily dispersible in water without surfactants, providing a simple route toward an aqueous conducting ink,[28] which has been used for printing a variety of MXene-based electronic devices (MXetronics[29]), manufacturing electrodes for epidermal electronics (MXtrodes[30]) and other applications.

In this work, we use MXene nanoparticles functionalized with a butylamine ligand[17] to form electronic devices and circuitry within insulating host liquids.[17] Aqueous MXene nanoparticles interact with butylamine ligands that are dissolved in toluene and assemble at the toluene–water interface. The resulting interfacial structures (including 2D films and 1D wires) have electrical conductance that is tunable via the original MXene dispersion concentration. We successfully demonstrate liquid wire electrical resistors, liquid electromechanical on/off switches, and non-volatile liquid photodetectors.

3. Results and Discussion

$Ti_3C_2T_x$ MXene flakes are prepared following previously published protocols[31] (see Experimental Section for details). Figure S1 (Supporting Information) shows a scanning electron microscopy (SEM) image of the MXene flakes deposited on an anodic aluminum oxide membrane. The flakes show lateral sizes of 1–10 μm, and the high transparency of the flakes indicates near complete delamination into single-layer sheets. UV–vis analysis of the synthesized MXene (Figure S2, Supporting Information) shows the expected plasmonic peak around 765 nm as well as several peaks in the UV range. Dynamic light scattering (DLS) measurements (Figure S3, Supporting Information) further deduce the average hydrodynamic size of 1700 nm, which can be correlated with the lateral size of the 2D flakes.[32] These MXene characteristics are in good agreement with previously reported values.[31] The flakes demonstrate negative surface charge with a measured zeta potential of −35 mV, which allows for the amine ligands in the complementary organic phase to drive the self-assembly of MXene flakes at the liquid–liquid interface following protonation of the ligand to the corresponding cationic ammonium salt.[17]

Figure 1 shows schematically the measurement configurations used to characterize the electrical properties of the self-assembled MXene films as well as an illustration of the jammed MXene film at the interface between water and toluene, with gold electrodes inserted to facilitate DC electrical conductance measurements. While in the present experiments we use toluene as the non-aqueous liquid component, self-assembly has been demonstrated in higher viscosity solvents such as silicone oil,[17] which can slow the self-assembly
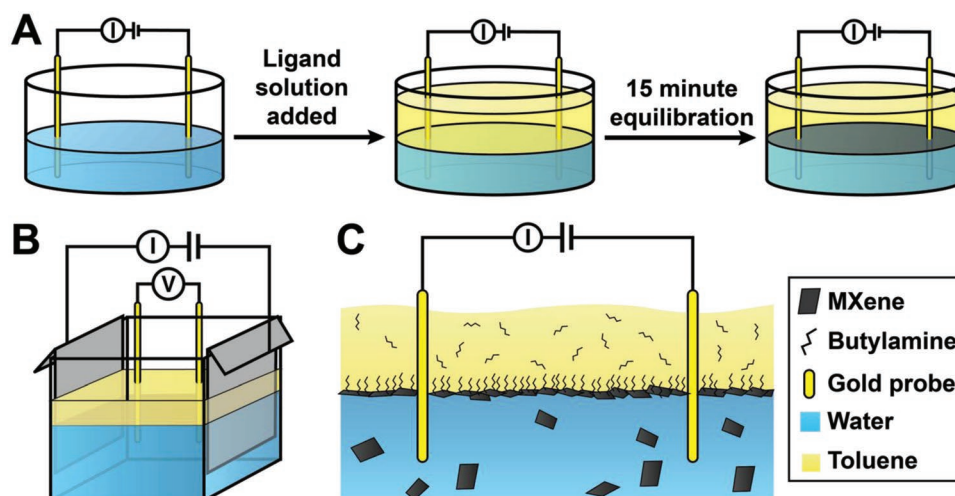
Figure 1. Schematic of electrical measurements at a biphasic interface. A) In the 2-probe configuration, the organic ligand solution (yellow) is gently layered over the aqueous MXene dispersion (blue). After a short time, an interfacial film is self-assembled around the probes allowing electrical percolation through the film. B) In the 4-probe configuration, parallel plates are used to create a uniform flow of current that can be detected by the central voltage probes, allowing a determination of sheet conductance. C) A schematic provides an idealized depiction of the initial experimental set up. Liquid toluene (yellow) containing butylamine ligands is deposited over water (blue) containing MXene nanoparticles. The conductive MXenes self-assemble at the interface and form a jammed, electrically conductive sheet. The electrical properties are probed via gold electrodes that pierce the sheet. Due to the miscibility of butylamine in water, it is expected that some butylamine will diffuse into the aqueous phase over time, but we see no evidence that this affects the relatively robust structural or electrical properties of the jammed conducting sheet.

process and alter the dynamics of 3D printed constructs, including those related to gravitational effects. In practice, we use both 2-probe (Figure 1A) and 4-probe (Figure 1B) measurement configurations. In the 4-probe configuration, the current injection/extraction probes are wide plates spanning the entire width of a rectangular cuvette, which quantifies the geometry and ensures a uniform current distribution throughout the jammed interface. After placing the probes and filling the sample dish with the aqueous MXene dispersion, the organic ligand solution is layered on top of the aqueous phase, creating a planar jammed interface (Figure 1C) while avoiding coating of the gold probes with the organic solvent to maintain good electrical contact.

Figure 2 shows room-temperature electrical conductance results for the jammed MXene 2D films. Figure 2A shows conductance versus time for several different concentrations of the aqueous MXene dispersion as the planar interface begins to equilibrate upon ligand addition under a fixed applied drive of 50 mV. This drive is chosen to avoid side reactions with the solvent (Figure S4, Supporting Information). As seen in the plot, with the increase in concentration of the MXene dispersion, the interface equilibrates more slowly but reaches a greater saturation conductance. Interfacial control interface experiments absent of MXenes or butylamine ligands, or of only water mixed with butylamine, show no electrical conductance, as expected. This establishes that interfacial jamming of the
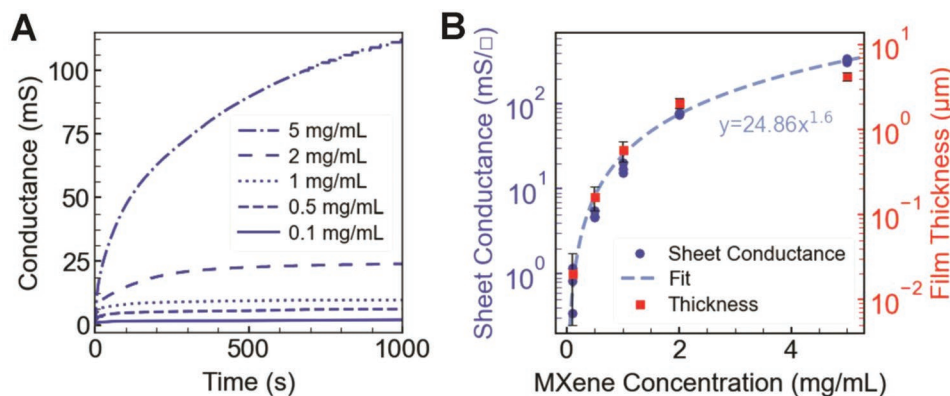
Figure 2. Room temperature electrical conductance measurements of jammed MXene nanoparticles at a biphasic interface. A) A plot of conductance versus time shows the equilibration of MXene films formed by various concentrations of the MXene dispersion. In this plot, ligands are added at time $t = 0$, marking the beginning of the 15 min equilibration. B) A plot of sheet conductance and film thickness versus MXene concentration shows a saturation of both conductance and thickness at high MXene concentrations of 5 mg mL^{-1}. The dashed line is a fit of Equation (1) to the conductance data (see main text).

MXene nanosheets is necessary and sufficient for establishing a conductive pathway, and that the electrical current is not due to, for example, ionic transport.

Measurements of the sheet conductance versus MXene concentration (Figure 2B) show that the conductance of the assembled films can be tuned by nearly three orders of magnitude by changing the concentration of the initial aqueous MXene dispersion. This tunability has immediate implications for liquid electronics as conductive interconnects and various resistors can be created with the same material system. The sheet conductance versus initial MXene dispersion concentration appears to follow a power law. In Figure 2B we plot as a blue dashed line the form

$$\sigma_{dc} = \sigma_o \left(c/c_0 \right)^\mu \qquad (1)$$

where $\sigma_o = 24.86$ mS, c/c_0 is the normalized concentration of the original MXene dispersion, and $\mu = 1.6$. The fit shows excellent agreement to the conductance data ($R^2 = 0.996$).

Equation (1) is reminiscent of the behavior of a percolation network, where the system connectivity t is given by

$$t = t_m \left(p - p_c \right)^\mu \qquad (2)$$

where t_m is the transfer integral for the basic network unit, p is the probability of bond formation between units, and p_c is the percolation probability threshold.[33–35] Indeed, the exponent $\mu = 1.6$ derived from the fit in Figure 2B is precisely that predicted from percolation theory for a system with dimensionality between 2 and 3.[33–35] Here, two obvious scenarios present themselves. In the first, the conducting MXene sheets quickly form as an imperfect conducting network but remain relatively fixed near monolayer thickness (perhaps as a double-layer, as has been observed for jammed systems of nano-clay platelets).[36] With increasing MXene dispersion concentration, "holes" in the quasi-2D sheet become progressively filled in, thus increasing the final dc electrical conductance per Equation (1). Alternatively, the percolation network could extend also in the out-of-plane direction; in this case the thickness of the films would increase with increasing MXene dispersion concentration leading to increased conductance.

In order to test these hypotheses, we characterize the thickness of the films. Because of technical challenges in measuring film thickness in situ (for example, the high optical light attenuation renders conventional interferometric methods ineffective), we determine the thickness of each established film by transferring it to a silicon wafer and then measuring the thickness via profilometry. As shown in Figure 2B, we find that the film thickness grows with increasing MXene dispersion concentration. The thicknesses range from 20 nm for the most dilute MXene dispersions to ≈4 μm for the highest MXene concentration. A series of representative profilometry traces (Figure S5, Supporting Information) shows how the film roughness increases with film thickness. These data indicate that the changes in conductance are likely due to varying thickness, rather than simply reducing gaps in a 2D "holey" MXene film. Interestingly, and as exemplified in Figure S6 (Supporting Information), the dc electrical conductance faithfully tracks the film thickness only up to moderate thicknesses (≈1 μm),

possibly due to internal ligand compression effects for thicker films.

The exceptional tunability in film geometry offers a powerful tool for different applications. In addition to tuning the electrical conductance of the films, the ability to change the thickness of the films far beyond a few unit layers has not been observed in other structured liquid systems and may be applied to create membranes of tunable permeation or for the preparation of thin films of arbitrary thickness. We observe that the thicker films are more mechanically robust during manipulation, offering the potential to tune the stiffness or durability of the films as well. The combination of electrical conductivity and tunable permeation in a single system could enable filtration or separation systems with integrated sensing capabilities.

We now turn to the creation of additional all-liquid electronic interconnects and devices as a proof of concept for liquid electronics. For these demonstrations, 2-probe contact configurations are employed using gold electrodes. We are motivated by previous work on other (non-electrically conducting) structured liquid systems, where tubes of an aqueous solvent with jammed nanoparticles at the surface have been 3D printed in arbitrary shapes in an organic ligand solution.[15–18] These works have demonstrated the range of complex geometries and line widths attainable via 3D printing of structured liquids. Here, we use similar printing to create tubular jammed MXene interconnect wires, resistors, switches, and sensors.

Figure 3 shows the creation and characterization of a tubular interconnect wire and break/make electromechanical switch. Figure 3A shows schematically the wire spanning the gold probes. For robust contacts, droplets of the aqueous MXene dispersion are placed around the gold electrodes prior to filling the container with the ligand solution (Figure 3A, left panel). A tubular wire is then printed spanning the droplets on the electrodes (Figure 3A, center panel). Figure S7 (Supporting Information) shows a printed wire spanning two probes to power an LED.

The printed tubular wire of Figure 3A, center panel, lends itself to create a reliable electromechanical switch. If the wire is ruptured, for example, by intentional mechanical cleavage, the wire fails to conduct (Figure 3A, right panel). If the cleaved ends of the wire are reconnected, either by mechanically manipulating the wire or by depositing a MXene-containing droplet over the break, the newly added MXenes self-assemble at the site of the break to reduce the interfacial tension between the solvents, repairing the jammed interface, and restoring the original conductance of the wire. This process will be identical to the original self-assembly process. Figure 3B shows the electrical results of such a repeated break/make/break cycle. The switching can be repeated, presumably indefinitely, with no degradation to the conductance as long as the dimensions (i.e., diameter, length) of the wire are preserved between cleavage/reformation cycles and the MXenes are protected from oxygen. As with traditional conductors, the conductance is dependent on the cross-section of the conductive material; maintaining the cross-sectional area upon reformation will restore the original value of the conductance. The ability to reform the liquid switch contrasts with conventional solid-state metal switches, where contacts invariably become worn or burned with repeated use.
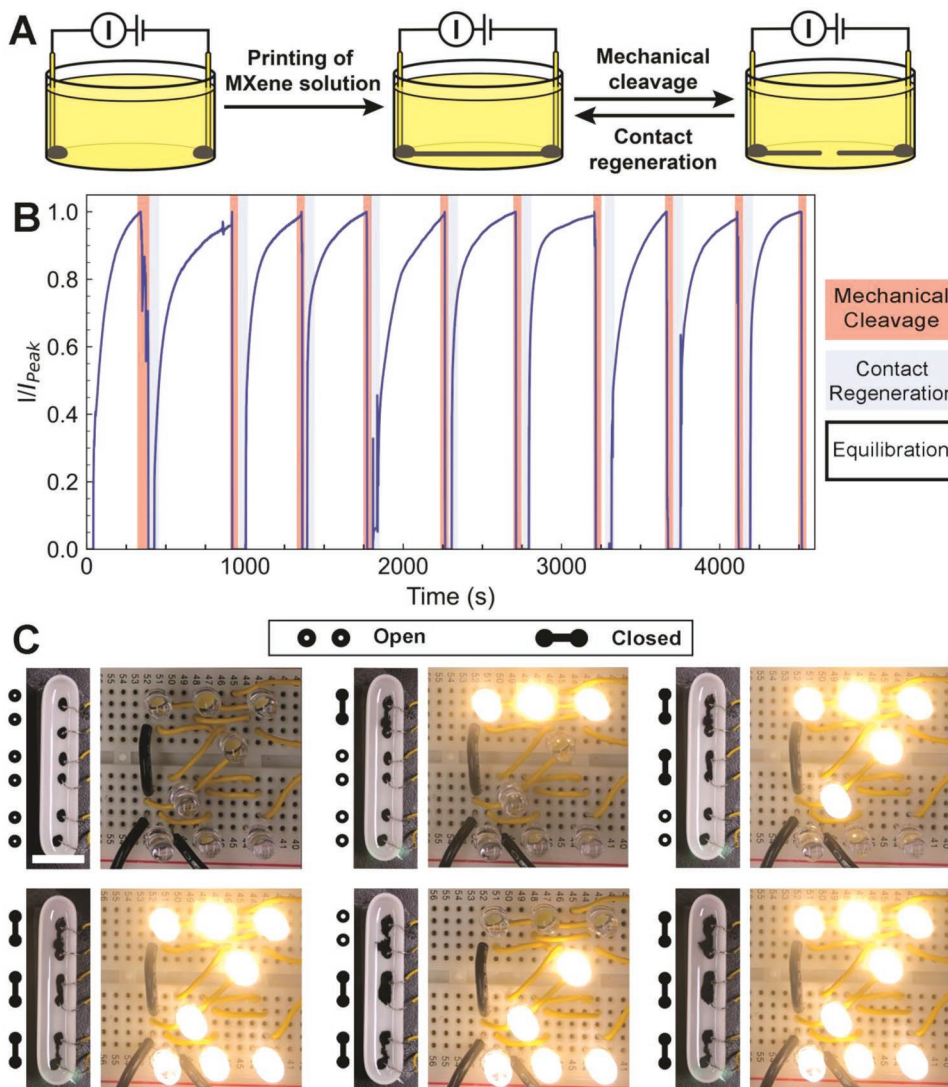
Figure 3. Creation of an electromechanical liquid switch using MXene wires. A) Schematic shows how tubular wires of MXenes can be printed between gold contacts in a 2-probe configuration and repeatedly cleaved/reformed through the addition of a small MXene droplet. In these experiments, an aqueous MXene dispersion is printed into a bath of toluene containing the butylamine ligand. The wire is printed along the bottom of the dish to facilitate easy mechanical cleavage. B) A long-duration experiment using the 2-probe configuration shows repeated opening and closing of the all-liquid switch, leading to electrical current off and on cycles. The time periods where the wire was cleaved, reformed by droplet addition or allowed to equilibrate are marked following the colored panels to the right of the plot. C) A set of MXene mechanical switches was then used to control the operation of an array of LEDs. The small inset to the left shows a picture of the three switches while the photos on the right show the LED response to each configuration. The uppermost switch controls the three LEDs in the top row; the middle switch controls the two center-most LEDs; and the bottom switch controls the three bottom-row LEDs. In the first panel (upper left), all three MXene switches are open and no LEDs are illuminated. In the second panel (upper center), the bottom MXene switch is closed, and selected LEDs are illuminated. In the third panel (upper right), the bottom two MXene switches are closed, and more LEDs are illuminated. In the fourth panel (bottom left), all three MXene switches are closed and all LEDs are illuminated. In the fifth and sixth panel, the bottom MXene switch is subsequently opened (bottom center) and again closed (bottom right), showing repeated switching control of the LEDs. Scalebar (white insert in top left panel of Figure 3C): 2 cm.

While we employed mechanical cleavage and addition of a new droplet of the MXene dispersion at the break, other forms of external stimuli could also be used to control the operation of the switch.

To highlight the efficacy of the printed MXene wire and switch, and the ability to integrate the MXene liquid wires with traditional solid-state electronics, we use a set of three MXene-based switches to control the operation of an array of LEDs (Figure 3C). As different MXene-based liquid tube switches are successively closed (and one reopened and again closed to show repeatability), different LED arrays are activated. In this device configuration, a liquid-based sensing platform allows an external mechanical stimulus to trigger a visual indicator. A circuit diagram for this device and a movie of the process are provided in the Supporting Information (Figure S8 and Movie S1, Supporting Information).

ADVANCED
SCIENCE NEWS

www.advancedsciencenews.com

ADVANCED
MATERIALS

www.advmat.de
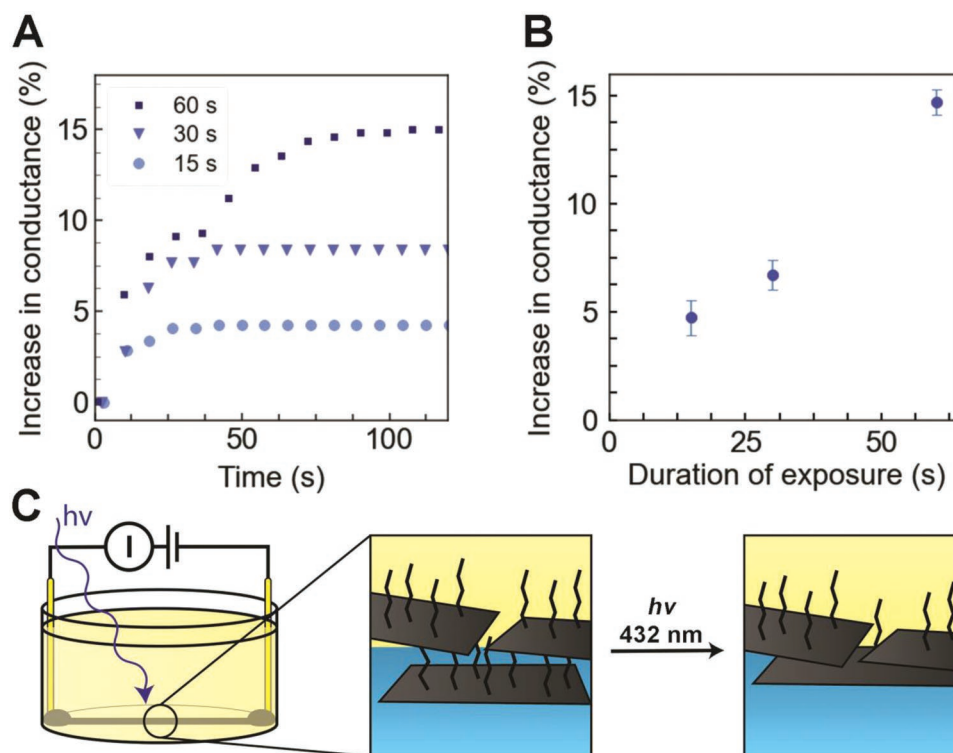
Figure 4. All-liquid non-volatile photodetector. A) Plot of change in conductance versus time as equilibrated MXene wires are irradiated by a 432 nm laser for various durations. In this plot, laser exposure begins at $t = 0$ and continues for 15, 30, or 60 s. This device serves as a non-volatile record of laser irradiation. The laser treatment can also be used to "dial in" a specified resistance for the MXene wire, thus reproducibly creating resistor components. The effect of the duration of laser exposure on the increase in conductance B) shows that various exposure times can be used to tailor the resistance of the wire. C) Cartoon schematic shows a possible scenario how laser irradiation displaces attached ligands, thereby bringing MXene sheets in closer proximity and permanently increasing the conductance of the printed wire.

The MXene wire platform can also be optically modulated using the plasmonic properties of MXenes.[37] Upon exposure of the MXene wires to a 432 nm laser, the conductance of the wires rapidly increases, as shown in **Figure 4**A. The effect of the duration of laser irradiation on the change in conductivity is also characterized (Figure 4B) indicating that a desired change can be selected by controlling the exposure time. We surmise that the absorbed light locally heats the flakes and displaces ligands separating adjacent MXene nanoparticles, thereby bringing the conducting MXene sheets closer together and increasing overall conductance (Figure 4C). Once the ligand-free nanoparticles are in close proximity, they do not easily unbind. Hence, this liquid-based optical sensor yields a non-volatile record of laser irradiation history. The local laser irradiation treatment serves another useful function: it can be used to tune or "dial in" the steady state electrical resistance of an MXene wire. Laser treatment allows resistors of a pre-determined resistance value to be locally created on the fly.

4. Conclusion

The ability to print desired architectures and carry charge along printed pathways in an all-liquid environment enables new opportunities in liquid electronics. In this work, we have used $Ti_3C_2T_x$ MXene nanosheets as a demonstration material,

but the chemistry of structured liquid systems is robust and may be extended to a variety of other conductive materials, including dozens of MXenes or blends of materials at the interface for additional functionality. The reconfigurability inherent to structured liquid systems may allow facile reprogramming or reconfiguring of circuits instead of fabricating new hard circuits from scratch. Implementation of this technology in consumer electronics admittedly will require additional engineering to address expected challenges of durability and lifetime, including oxygen contamination, volatilization, acoustic vibrations, and thermal degradation. Remedies may include suitable encapsulation, addition of oxygen scavengers, and viscosity engineering. Nevertheless, the work reported here lays the fundamental groundwork for the creation of liquid electronic components. In addition, the ability to electrify an interface or tube while allowing reagents to flow through the tube and across interfacial membranes[16,38] could have applications in catalysis and microfluidics, especially in systems where the product and substrate have affinity for solvents of differing polarity.

5. Experimental Section

General: Unless specified, materials were obtained from a commercial supplier and unmodified before use. A Nordson EFD Ultimus II

pneumatic pump was used to dispense the aqueous MXene dispersion for experiments using printed MXene wires.

Synthesis of MXene Nanosheets: Synthesis of $Ti_3C_2T_x$ MXene was performed according to the previously published procedure.[31] To synthesize Ti_3AlC_2 MAX precursor, TiC, Ti, and Al powders with the mass ratio of TiC:Ti:Al = 2:1:1 were mixed via ball milling with zirconia balls, followed by annealing at 1380 °C for 2 h under Ar atmosphere. The resultant material was powdered and washed with 9 M HCl overnight to remove the metallic impurities, then sieved to obtain particles below 38 μm in size. To synthesize $Ti_3C_2T_x$ MXene, 1 g of the MAX precursor was added to 20 mL of a solution containing a mixture of HF (49%, 2 mL), HCl (36%, 12 mL), and H_2O (6 mL) and stirred for 24 h at 35 °C. After the reaction was complete, MXene was washed with water until neutral pH via several cycles of centrifugation. The obtained multilayer MXene was mixed with 1 g of LiCl in 50 mL of water for 18 h. The MXene/LiCl mixture was washed with water via repeated cycles of centrifugation (15 min, 3500 rpm). After the second centrifugation cycle, the dark supernatant containing single-layer MXene flakes was collected, concentrated using high-speed centrifugation (10 min, 10000 rpm), and stored in an Ar-sealed vial at 4 °C. Size distributions of the MXene nanoflakes were polydisperse with lateral dimensions between 1.3–1.6 μm.

Preparation of MXene Ink and Ligand Solution: The concentration of the stock MXene solution was determined by taking an aliquot solution and measuring the mass after drying it overnight in a vacuum at 50 °C. To prepare a MXene dispersion for printing, the concentrated MXene solution was diluted to 2 mg mL^{-1} with milli-Q water. The inks were used within several hours to avoid degradation of the flakes by oxidation. The ligand solution was made by adding 5% (w/w) of butylamine into toluene. The solution was inverted ≈20 times to ensure proper mixing before use.

DC Conductivity Measurements: A Keithley 2400 SourceMeter was used for all DC measurements. The gold probes were cut to size from commercially available gold wires (99.999%), while the foils used for 4-point measurements were cut to size from platinum foil (99.999%). 2-probe measurements were conducted with an applied potential of 50 mV to avoid side reactions in the solvents.

For 4-probe measurements (used for sheet conductance measurements), a square glass dish (lateral dimension = 2 cm) was used to contain the solutions. Platinum foils at opposite sides of the square dish were used to supply a current of ±100 μA, while gold probes located in the equipotential region were used to measure the induced voltage. With the probes in place, the bottom of the dish was filled with 3 mL of the aqueous MXene dispersion. The measurement was then started and 2 mL of the ligand solution was gently layered on top with a pipette.

For measurements of the printed MXene wires, a 2-probe configuration was used. For these measurements, the probes were placed at the edges of the dish and droplets of the MXene dispersion were placed around the base of the probes. The dish was then filled with ≈4 mL of the 5% (w/w) butylamine in toluene ligand solution and the measurement was started. A Nordson EFD pneumatic pump was used to print a tube of the MXene dispersion between the preplaced droplets. Typical forward and reverse pressures were 0.7 psi and 3 inches H_2O. Note that droplets of the MXene must be placed around the probes before filling the container with the ligand solution to avoid poor electrical contact between the probes and the self-assembled interface.

Profilometry: A Datek profilometer with 12.5 μm stylus and 1 mg force was used to measure the MXene film thickness. Numerous scratches to the silicon substrate were included in a 5 mm scan enabling accurate leveling of the profile. Film thickness was calculated by averaging the micron scale roughness. Thinned material near the edges of the substrate was excluded from the average measurement.

Laser Heating: For laser irradiation experiments, a 2 W 432 nm handheld laser was used for irradiation of the printed MXene wire. The MXene wire was printed and allowed to equilibrate for ≈15 min. The laser was switched on for a fixed duration while continuously measuring the current under a constant drive of 50 mV.

Supporting Information

Supporting Information is available from the Wiley Online Library or from the author.

Conflict of Interest

The authors declare no conflict of interest.

Data Availability Statement

The data that support the findings of this study are available from the corresponding author upon reasonable request.

[1] J. Cui, L. Zhang, *J. Hazard. Mater.* **2008**, *158*, 228.

[2] K. Huang, J. Guo, Z. Xu, *J. Hazard. Mater.* **2009**, *164*, 399.

[3] A. Behnamfard, M. M. Salarirad, F. Veglio, *Waste Manage.* **2013**, *33*, 2354.

[4] D. Akinwande, N. Petrone, J. Hone, *Nat. Commun.* **2014**, *5*, 5678.

[5] S. Kabiri Ameri, R. Ho, H. Jang, L. Tao, Y. Wang, L. Wang, D. M. Schnyer, D. Akinwande, N. Lu, *ACS Nano* **2017**, *11*, 7634.

[6] H. Li, Y. Ma, Y. Huang, *Mater Horiz* **2021**, *8*, 383.

[7] Y. Zhu, J. Liu, T. Guo, J. J. Wang, X. Tang, V. Nicolosi, *ACS Nano* **2021**, *15*, 1465.

[8] X. Li, X. Li, H. Li, Y. Zhao, J. Wu, S. Yan, Z. Yu, *Adv. Funct. Mater.* **2022**, *32*, 2110636.

[9] J. Wissman, M. D. Dickey, C. Majidi, *Adv. Sci.* **2017**, *4*, 1700169.

[10] Y. Chen, Z. Liu, D. Zhu, S. Handschuh-Wang, S. Liang, J. Yang, T. Kong, X. Zhou, Y. Liu, X. Zhou, *Mater. Horiz.* **2017**, *4*, 591.

[11] L. Teng, S. Ye, S. Handschuh-Wang, X. Zhou, T. Gan, X. Zhou, *Adv. Funct. Mater.* **2019**, *29*, 1808739.

[12] G. Li, F. Sun, H. Chen, Y. Jin, A. Zhang, J. Du, *ACS Appl. Mater. Interfaces* **2021**, *13*, 56961.

[13] M. S. Kim, S. Kim, J. Choi, S. Kim, C. Han, Y. Lee, Y. Jung, J. Park, S. Oh, B.-S. Bae, H. Lim, I. Park, *ACS Appl. Mater. Interfaces* **2022**, *14*, 1826.

[14] M. Cui, T. Emrick, T. P. Russell, *Science* **2013**, *342*, 460.

**ADVANCED
SCIENCE NEWS**

www.advancedsciencenews.com

**ADVANCED
MATERIALS**

www.advmat.de

[15] J. Forth, X. Liu, J. Hasnain, A. Toor, K. Miszta, S. Shi, P. L. Geissler, T. Emrick, B. A. Helms, T. P. Russell, *Adv. Mater.* **2018**, *30*, 1707603.

[16] G. Xie, J. Forth, Y. Chai, P. D. Ashby, B. A. Helms, T. P. Russell, *Chem* **2019**, *5*, 2678.

[17] J. D. Cain, A. Azizi, K. Maleski, B. Anasori, E. C. Glazer, P. Y. Kim, Y. Gogotsi, B. A. Helms, T. P. Russell, A. Zettl, *ACS Nano* **2019**, *13*, 12385.

[18] D. Lin, T. Liu, Q. Yuan, H. Yang, H. Ma, S. Shi, D. Wang, T. P. Russell, *ACS Appl. Mater. Interfaces* **2020**, *12*, 55426.

[19] X. Liu, N. Kent, A. Ceballos, R. Streubel, Y. Jiang, Y. Chai, P. Y. Kim, J. Forth, F. Hellman, S. Shi, D. Wang, B. A. Helms, P. D. Ashby, P. Fischer, T. P. Russell, *Science* **2019**, *365*, 264.

[20] B. Qian, S. Shi, H. Wang, T. P. Russell, *ACS Appl. Mater. Interfaces* **2020**, *12*, 13551.

[21] A. Iqbal, F. Shahzad, K. Hantanasirisakul, M.-K. Kim, J. Kwon, J. Hong, H. Kim, D. Kim, Y. Gogotsi, C. M. Koo, *Science* **2020**, *369*, 446.

[22] A. VahidMohammadi, J. Rosen, Y. Gogotsi, *Science* **2021**, *372*, eabf1581.

[23] S. Shi, B. Qian, X. Wu, H. Sun, H. Wang, H. Zhang, Z. Yu, T. P. Russell, *Angew. Chem., Int. Ed.* **2019**, *58*, 18171.

[24] S. Zhao, L. Li, H.-B. Zhang, B. Qian, J.-Q. Luo, Z. Deng, S. Shi, T. P. Russell, Z.-Z. Yu, *Mater. Chem. Front.* **2020**, *4*, 910.

[25] M. Alhabeb, K. Maleski, B. Anasori, P. Lelyukh, L. Clark, S. Sin, Y. Gogotsi, *Chem. Mater.* **2017**, *29*, 7633.

[26] A. Lipatov, A. Goad, M. J. Loes, N. S. Vorobeva, J. Abourahma, Y. Gogotsi, A. Sinitskii, *Matter* **2021**, *4*, 1413.

[27] S. Wan, X. Li, Y. Chen, N. Liu, Y. Du, S. Dou, L. Jiang, Q. Cheng, *Science* **2021**, *374*, 96.

[28] C. Zhang, L. McKeon, M. P. Kremer, S.-H. Park, O. Ronan, A. Seral-Ascaso, S. Barwich, C. Ó. Coileáin, N. McEvoy, H. C. Nerl, B. Anasori, J. N. Coleman, Y. Gogotsi, V. Nicolosi, *Nat. Commun.* **2019**, *10*, 1795.

[29] H. Kim, H. N. Alshareef, *ACS Mater. Lett.* **2020**, *2*, 55.

[30] N. Driscoll, B. Erickson, B. B. Murphy, A. G. Richardson, G. Robbins, N. V. Apollo, G. Mentzelopoulos, T. Mathis, K. Hantanasirisakul, P. Bagga, S. E. Gullbrand, M. Sergison, R. Reddy, J. A. Wolf, H. I. Chen, T. H. Lucas, T. R. Dillingham, K. A. Davis, Y. Gogotsi, J. D. Medaglia, F. Vitale, *Sci. Transl. Med.* **2021**, *13*, abf8629.

[31] T. S. Mathis, K. Maleski, A. Goad, A. Sarycheva, M. Anayee, A. C. Foucher, K. Hantanasirisakul, C. E. Shuck, E. A. Stach, Y. Gogotsi, *ACS Nano* **2021**, *15*, 6420.

[32] K. Maleski, C. E. Ren, M.-Q. Zhao, B. Anasori, Y. Gogotsi, *ACS Appl. Mater. Interfaces* **2018**, *10*, 24491.

[33] S. Havlin, D. Ben-Avraham, *Adv. Phys.* **1987**, *36*, 475.

[34] A. L. Efros, B. I. Shklovskii, *Phys. Stat. Sol.* **1976**, *76*, 475.

[35] R. B. Pandey, D. Stauffer, *Phys. Rev. Lett.* **1983**, *51*, 527.

[36] W. Feng, Y. Chai, J. Forth, P. D. Ashby, T. P. Russell, B. A. Helms, *Nat. Commun.* **2019**, *10*, 1095.

[37] K. Maleski, C. E. Shuck, A. T. Fafarman, Y. Gogotsi, *Adv. Optical Mater.* **2021**, *9*, 2001563.

[38] Y. Tang, W. Cheng, *Nanoscale* **2015**, *7*, 16151.